Run plan for $^{15}\mathrm{N}(p,\alpha_1\gamma)^{12}\mathrm{C}$ angular distribution measurements

August 30, 2018

1 Introduction

The $^{15}\mathrm{N}(p,\alpha_1\gamma)^{12}\mathrm{C}$ reaction is familiar to anyone who has done proton induced γ-ray spectroscopy. While $^{15}\mathrm{N}$ makes up only about 0.364(20)% of naturally occurring nitrogen, it is nearly impossible to remove all traces of nitrogen from most targets. Since the reaction is a nuclear type reaction, it is often several orders of magnitude larger in cross section than any capture reaction. Further, despite populating the first excited state in $^{12}\mathrm{C}$ at $E_x = 4.44$ MeV, the reaction has a positive Q-value of 0.52 MeV, giving it a high cross section even at very low energies.

In addition to being an annoyance for γ-ray spectroscopy, the reaction is also very useful in material science. Since the reaction has such a high cross section, any thin film containing $^{15}\mathrm{N}$ can be subjected to nuclear reaction analysis NRA in order to obtain information about the amount of nitrogen as a function of depth (usually on the few to a few 10's of nanometers scale). While the α-particles that are produced from the reaction can not escape the infinitely thick targets, the 4.44 MeV γ-ray easily can. See, for example, Ref. [4]. KTM: This reaction seems to be often used in inverse kinematics to scan hydrogen density profiles in solid materials as well [1].

For nuclear astrophysics applications, the $^{15}\mathrm{N}(p,\alpha_1\gamma)^{12}\mathrm{C}$ reaction is not directly an important reaction for nucleosynthesis or energy production. The $^{15}\mathrm{N}(p,\alpha)^{12}\mathrm{C}$ reaction is critical part of the carbon-nitrogen-oxygen cycle, but at the low temperatures (corresponding to about 20 keV center of mass energy) where this hydrogen burning cycle is important, the ground state $^{15}\mathrm{N}(p,\alpha_0)^{12}\mathrm{C}$ cross section heavily dominates. However, the $^{15}\mathrm{N}(p,\alpha_1\gamma)^{12}\mathrm{C}$ is very helpful indirectly, because it provides an easily measurable alternative method to probe the level structure of the $^{16}\mathrm{O}$ compound nucleus. The reaction can be included in a unitary global nuclear model to constrain the decay probability to this channel. This is a fancy way of saying that in order to accurately constrain the model, you need to know the decay branchings as a function of energy for each way in which the nucleus can decay.

In the 1950's this reaction saw a lot of attention as it was both easy to measure, thanks to its high cross section, and is a probe of some interesting

nuclear structure [8, 2, 3]. In particular, there are two unnatural parity states at $E_x = 12.530(1)$ and 12.9686(4) MeV in the ^{16}O compound nucleus. Because these states are of unnatural parity, angular momentum and parity conservation dictates that α-decay to the ground state of ^{16}O is forbidden (that is, highly suppressed, although not impossible). Since these two states, both $J^\pi = 2^-$ are both close to the proton and α_1 thresholds, Coulomb penetrability also implies that their decay widths must be rather small. This has the practical result that these states show up as narrow resonances at $E_p = 430$ and 897 keV in both the $^{15}\mathrm{N}(p,\alpha_1)^{12}\mathrm{C}$ and $^{15}\mathrm{N}(p,p)^{15}\mathrm{N}$ reactions. Their *reduced* proton widths (or proton spectroscopic factors) are rather large so they show up in both reactions as strong resonances as shown in Fig. 1. In a recent publication by [10] these resonance strengths are summarized and new measurements were made. However, in this work the strength for the $E_p = 897$ keV is found to be considerably different than previous measurements. In addition, the angular distributions reported by [10] for both resonances are inconsistent with symmetry about 90°, making their results questionable. This is a point of interest for a future study.

2 Efficiency calibration and target thickness determination

The $^{15}\mathrm{N}(p,\alpha_1\gamma)^{12}\mathrm{C}$ cross section can be measured in a straight-forward manner thanks to some nice features of the cross section and to some careful previous work. The cross section above $E_p \approx 0.8$ MeV becomes rather large, always greater than 1 mb at higher observed energies. There is also a narrow resonance at $E_p = 897$ keV ($E_x = 12.9686(4)$ MeV, $J^\pi = 2^-$) that has been well studied and both the γ-ray angular distribution (see Fig. 2) and strength (see Table 1) are known.

The targets that will be utilized are those from the experiment reported in [9, 7]. The targets are made of a thin layer of titanium nitride on a thick titanium backing. The targets have shown to have very favorable properties that include a very well defined, constant stoichiometry, layering of TiN, that is, no nitrogen has diffused into the deeper layers of the Ti backing. The target that will be used is the one used previously at Notre Dame that has seen 5 C of total beam on target and had nearly no signs of deterioration. The thickness of this target was measured to be 7.2(3) keV at the $E_p = 429$ keV resonance in the $^{15}\mathrm{N}(p,\alpha_1\gamma)^{12}\mathrm{C}$ reaction.

The target thickness will be remeasured by a repeated measurement of the thick target yield over the $E_p = 430$ keV resonance (see Fig. 2) of [9]. If the yield from this low energy resonance is too low, the $E_p = 897$ keV resonance can be used instead. The efficiency can then be determined from the known strength of the resonance and the target stoichiometry. A rate estimate is given below.

In the 1 mb total cross section region, on average, it will take 1.4 hours to detect 1000 counts with a 1 μA beam on target.

Figure 1: All known angular distribution measurements of the $^{15}\mathrm{N}(p,\alpha_1\gamma)^{12}\mathrm{C}$ cross section over the region from threshold up to $E_p \approx 2$ MeV. The measurements of [5] are the only ones made in off-resonance regions. The red solid line indicates an R-matrix calculation using the level parameters reported in [6], which are in good agreement with the data.

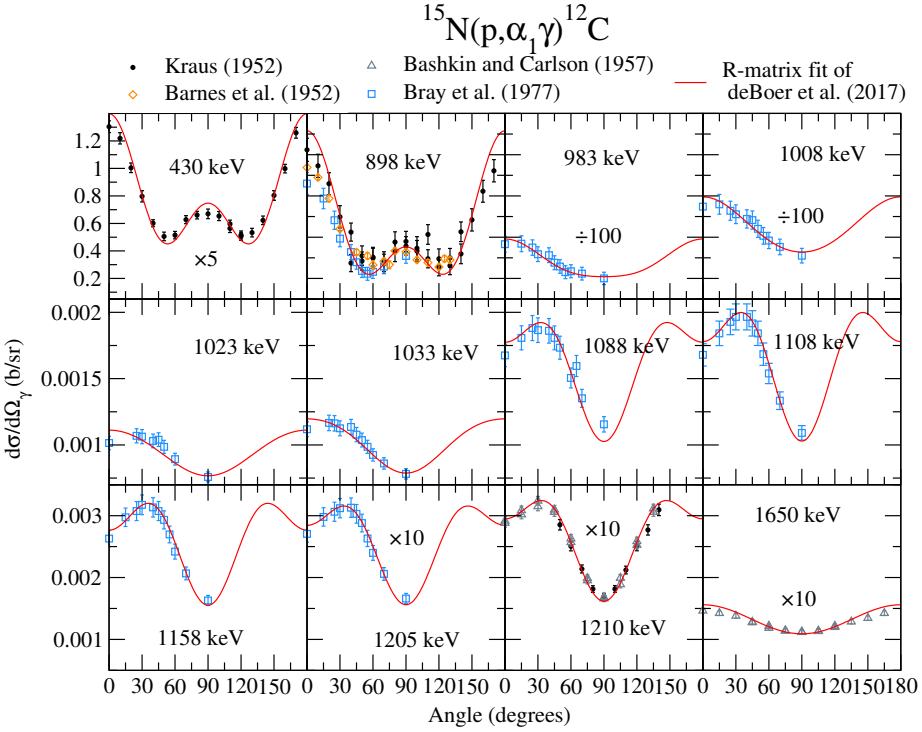

Table 1: Summary of resonance properties for the two narrow low energy resonances in the $^{15}\mathrm{N}(p,\alpha_1\gamma)^{12}\mathrm{C}$ cross section.

		$\omega\gamma$ (eV)	
E_p (keV)	$\Gamma_{c.m.}$ (keV)	Literature	[10]
430	0.111(10)	21.1(14) [4]	22.7(14)
897	1.34(4)	293(38) [11]	362(20)

Figure 2: Calculation of the $^{15}\mathrm{N}(p,\alpha_1\gamma)^{12}\mathrm{C}$ cross section based on the global R-matrix fit from [6] (red solid line). The vertical dashed lines black lines indicate energies at which angular distribution measurements have been made by [8, 2, 3, 5].

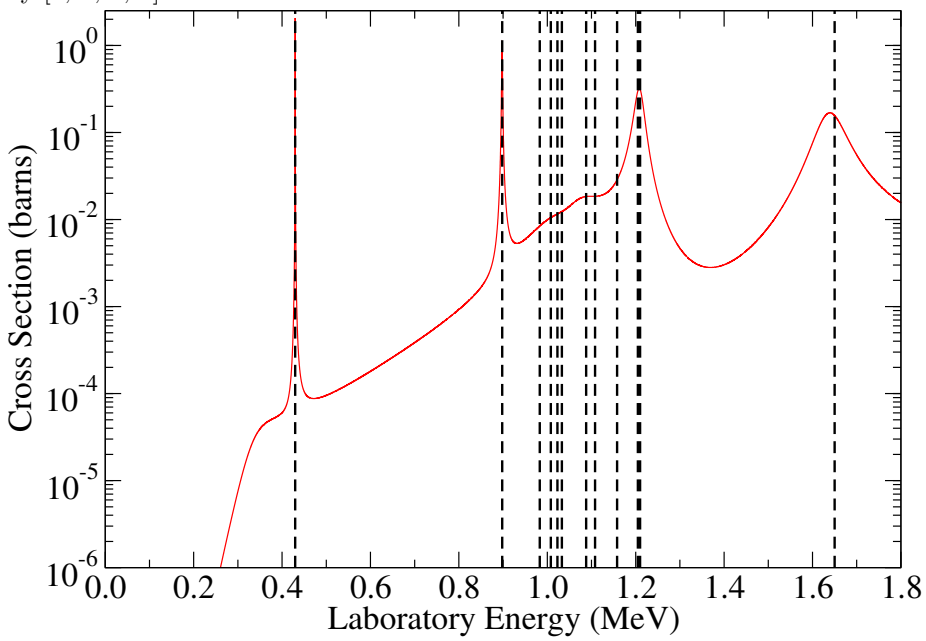

- 25 $\mu g/cm^2$ Thick TiN target: $(2.4 \times 10^{17}\ {}^{15}\mathrm{N}/cm^2)$
  - 7 keV thick at 430 keV
  - 4 keV thick at 1 MeV
  - 2 keV thick at 3 MeV
- Take limiting case of average differential cross section: $\frac{d\sigma}{d\Omega} \approx \frac{\sigma}{4\pi} \approx \frac{1\ mb}{4\pi\ Sr}$
- Solid Angle: 22.5 mSr
  - For a target-detector distance $d = 30\ cm$
  - Detector radius $r = 1\ inch$
- Using the thin target yield formula:

$$\begin{aligned}\frac{Y}{s} &= \epsilon \frac{d\sigma}{d\Omega} \delta\Omega N_t \frac{N_b}{s} \\ &\approx (0.07)\left(\frac{1\ mb}{4\pi\ Sr}\right)(0.0225\ Sr)\left(2.4 \times 10^{17}\ \frac{{}^{15}\mathrm{N}}{cm^2}\right)\left(\frac{10^{-27}\ cm^2}{mb}\right)\left(\frac{10^{-6}}{1.6 \times 10^{-19}}\frac{I}{1\ \mu A}\right) \\ &\approx \boxed{0.18\ Hz\left(\frac{I}{1\ \mu A}\right)\left(\frac{\sigma}{1\ mb}\right)}\end{aligned}$$

3 Run Plan

The run is divided into three main parts:

1. Thick target yield scan of $E_p = 430$ and 897 keV resonances.
2. Off-resonance measurements at energies of previous measurements with additional measurements in the 1.2 to 1.6 MeV range.
3. On and off-resonance measurements in the higher energy region up to 4 MeV.

Note: Since the beam energy needs to be well defined, recycle the magnet whenever you go up in energy.

Note: There is only one γ-ray line of interest at 4.44 MeV. When a number of counts is referenced, it is with respect to the area of this peak.

3.1 Narrow resonance scans

Locate resonance at $E_p = 430$ keV. In [9], the front edge of the resonance was found to be at about 429 keV and had a flat top that when down to about 434 keV. A high energy tail was observed that extended up to about 439 keV. See Fig. 3 that has been taken from Fig. 2 of [9].

Figure 3: Example thick target yield curve scan of the 430 keV resonance from [9].

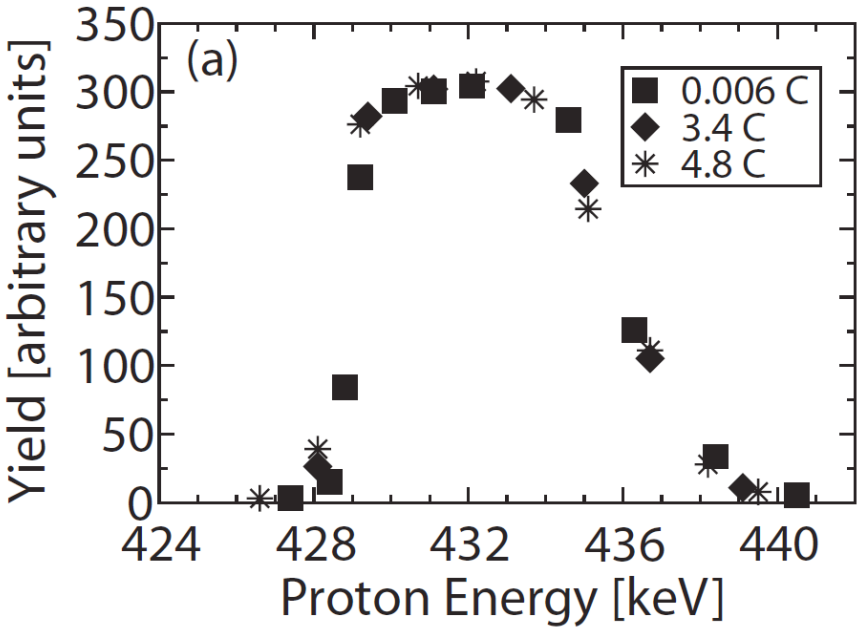

Begin the scan at about $E_p = 441$ keV and step down in 0.5 keV steps until you think you are approaching the front edge. Obtain 1000 counts in 30∘ detector for each energy step. Then try to step down the front edge in 0.1 keV steps. After resonance scan is complete, recycle the magnet and return to center of plateau region. Perform long run on top of resonance and get at least 2000 counts in all detectors. Lowest count rate detectors should be those at 45 and 60°.

Repeat the same procedure for the $E_p = 879$ keV resonance. Start at about $E_p = 910$ keV and scan down in 0.5 keV steps. When you reach the front edge try to step down in 0.1 keV steps. Obtain 1000 counts in 30° detector for each run. When finished with resonance scan go back to center of plateau region and do a long run until you have at least 2000 counts for each detector. Again, the lowest yields will be in the 45 and 60° degree detectors.

3.2 Off-resonance measurements below 2 MeV

The general form of the cross section below $E_p = 2$ MeV is shown in Fig. 2. In this region the energies of [5] will be repeated and new measurements will be made at some additional energies as given in Table 2.

Table 2: Energies for measurements in the low energy region. The measurements of [5] will all be repeated. Energies are quoted so that the effective energy ($E_p - \delta E = E_{eff}$), where E_p is the beam energy, δE is half the energy loss through the target, and E_{eff} is the corrected average energy.

E_p (keV)	(N)ew or (R)epeated
966	N
986	R
1011	R
1026	R
1036	R
1064	N
1091	R
1111	R
1136	N
1161	R
1185	N
1208	R
1213	R
1238	N
1263	N
1313	N
1363	N
1413	N
1463	N
1513	N
1563	N
1613	N
1652	R
1700	N
1800	N
1900	N
1940	N
1950	N
1960	N
1970	N
1980	N
1985	R
1990	N
2000	N

3.3 Measurements above 2 MeV

In the region above 2 MeV on-resonance angular distributions have been made by [3] and a 0° excitation curve is shown in Fig. 4. Energies to be measured are given in Table 3.

4 Rate Estimate for $^{nat}\mathrm{Zn}(p,x)^{66}\mathrm{Ga}$ calibration source production

- Using 10 MeV Protons (10 MeV - 3.1 MeV)
  - 300 μm Range for 10 MeV protons in Zinc
  - 3.1 MeV residual energy after traversing the target.
- 0.010" Thick Zinc Sheet
  - 254 μm
  - 181.3 mg/cm^2

References

[1] 15n hydrogen profiling: Scientific applications. *Nuclear Instruments and Methods*, 149(1):1 – 8, 1978.

[2] C. A. Barnes, D. B. James, and G. C. Neilson. Angular distribution of the gamma rays from the reaction $^{15}\mathrm{N}(p,\alpha\gamma)^{12}\mathrm{C}$. *Canadian Journal of Physics*, 30(6):717–718, 1952.

[3] S. Bashkin and R. R. Carlson. Gamma rays from the proton bombardment of N^{15}. *Phys. Rev.*, 106:261–266, Apr 1957.

[4] H. W. Becker, M. Bahr, M. Berheide, L. Borucki, M. Buschmann, C. Rolfs, G. Roters, S. Schmidt, W. H. Schulte, G. E. Mitchell, and J. S. Schweitzer. Hydrogen depth profiling using ^{18}O ions. *Zeitschrift für Physik A Hadrons and Nuclei*, 351(4):453–465, Dec 1995.

[5] K. Bray, A. Frawley, T. Ophel, and F. Barker. Levels of ^{16}O near 13 MeV excitation from $^{15}\mathrm{N} + p$ reactions. *Nuclear Physics A*, 288(2):334 – 350, 1977.

[6] R. J. deBoer, J. Görres, M. Wiescher, R. E. Azuma, A. Best, C. R. Brune, C. E. Fields, S. Jones, M. Pignatari, D. Sayre, K. Smith, F. X. Timmes, and E. Uberseder. The $^{12}\mathbf{C}(\alpha,\gamma)^{16}\mathbf{O}$ reaction and its implications for stellar helium burning. *Rev. Mod. Phys.*, 89:035007, Sep 2017.

Figure 4: Excitation curve of high energy region from [3].

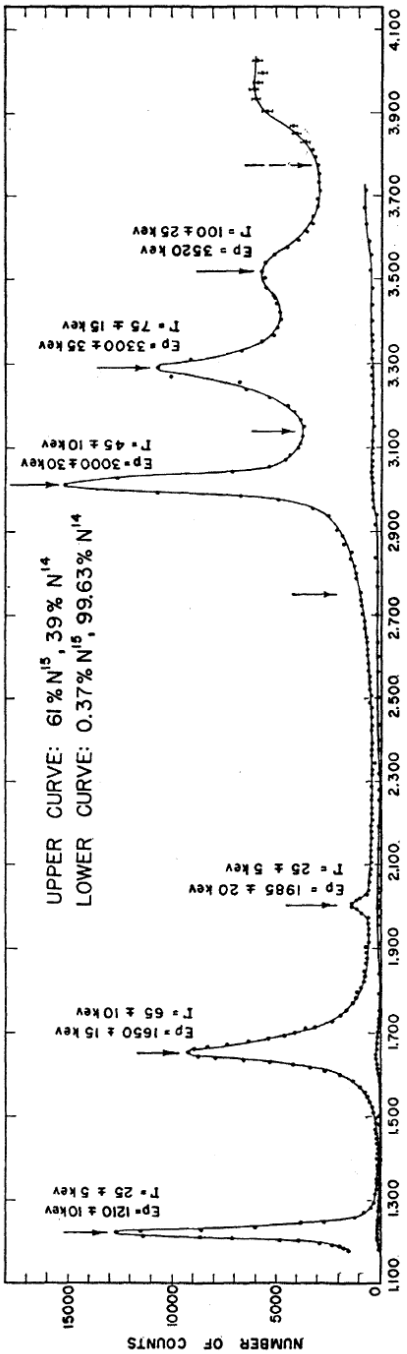

FIG. 2. Yields of 4.43-Mev gamma rays at 0° from proton bombardment of nitrogen gas targets. Standard deviation is shown where it exceeds the size of point. Average peak positions and widths are given. Solid arrows indicate positions at which angular distributions were measured. Dashed arrow indicates observed position of pn threshold.

Table 3: Energies for measurements in the high energy region. The measurements of [3] will all be repeated. Energies are quoted so that the effective energy ($E_p - \delta E = E_{eff}$), where E_p is the beam energy, δE is half the energy loss through the target, and E_{eff} is the corrected average energy.

E_p (keV)	(N)ew or (R)epeated	E_p (keV)	(N)ew or (R)epeated
2010	N	3430	N
2020	N	3460	N
2030	N	3490	N
2040	N	3500	N
2100	N	3510	N
2200	N	3520	R
2300	N	3530	N
2400	N	3550	N
2500	N	3600	N
2600	N	3650	N
2700	N	3700	N
2750	R	3900	N
2800	N	3950	N
2900	N	4000	N
2920	N		
2940	N		
2960	N		
2980	N		
2990	N		
3000	R		
3010	N		
3020	N		
3040	N		
3060	N		
3080	N		
3100	N		
3130	R		
3150	N		
3200	N		
3250	N		
3270	N		
3280	N		
3290	N		
3300	R		
3310	N		
3320	N		
3340	N		
3360	N		
3400	N		

[7] G. Imbriani, R. J. deBoer, A. Best, M. Couder, G. Gervino, J. Görres, P. J. LeBlanc, H. Leiste, A. Lemut, E. Stech, F. Strieder, E. Uberseder, and M. Wiescher. Measurement of γ rays from ^{15}N(p,γ)^{16}O cascade and ^{15}N(p,$\alpha_1\gamma$)^{12}C reactions. *Phys. Rev. C*, 85:065810, Jun 2012.

[8] A. A. Kraus, A. P. French, W. A. Fowler, and C. C. Lauritsen. Angular distribution of gamma-rays and short-range alpha-particles from ^{15}N($p, \alpha\gamma$)^{12}C. *Phys. Rev.*, 89:299–301, Jan 1953.

[9] P. J. LeBlanc, G. Imbriani, J. Görres, M. Junker, R. Azuma, M. Beard, D. Bemmerer, A. Best, C. Broggini, A. Caciolli, P. Corvisiero, H. Costantini, M. Couder, R. deBoer, Z. Elekes, S. Falahat, A. Formicola, Z. Fülöp, G. Gervino, A. Guglielmetti, C. Gustavino, G. Gyürky, F. Käppeler, A. Kontos, R. Kuntz, H. Leiste, A. Lemut, Q. Li, B. Limata, M. Marta, C. Mazzocchi, R. Menegazzo, S. O'Brien, A. Palumbo, P. Prati, V. Roca, C. Rolfs, C. Rossi Alvarez, E. Somorjai, E. Stech, O. Straniero, F. Strieder, W. Tan, F. Terrasi, H. P. Trautvetter, E. Uberseder, and M. Wiescher. Constraining the S factor of ^{15}N(p, γ)^{16}O at astrophysical energies. *Phys. Rev. C*, 82:055804, Nov 2010.

[10] M. Marta, E. Trompler, D. Bemmerer, R. Beyer, C. Broggini, A. Caciolli, M. Erhard, Z. Fülöp, E. Grosse, G. Gyürky, R. Hannaske, A. R. Junghans, R. Menegazzo, C. Nair, R. Schwengner, T. Szücs, S. Vezzú, A. Wagner, and D. Yakorev. Resonance strengths in the ^{14}N(p,γ)^{15}O and ^{15}N(p,$\alpha\gamma$)^{12}C reactions. *Phys. Rev. C*, 81:055807, May 2010.

[11] F. Zijderhand and C. van der Leun. Strong M2 transitions. *Nuclear Physics A*, 460(2):181 – 200, 1986.